Article

Electrochemical and Computational Insights into the Reduction of [Fe$_2$(CO)$_6${μ-(SCH$_2$)$_2$GeMe$_2$}] Hydrogenase H-Cluster Mimic

Hassan Abul-Futouh [1], **Wolfgang Imhof [2,*]**, **Wolfgang Weigand [3,*]** and **Laith R. Almazahreh [3,4,*]**

[1] Department of Pharmacy, Al-Zaytoonah University of Jordan, P.O. Box 130, Amman 11733, Jordan; h.abulfutouh@zuj.edu.jo

[2] Institut für Integrierte Naturwissenschaften, Universität Koblenz-Landau, Universitätsstr. 1, D-56070 Koblenz, Germany

[3] Institut für Anorganische und Analytische Chemie, Friedrich-Schiller-Universität Jena, Humboldt Str. 8, 07743 Jena, Germany

[4] ERCOSPLAN Ingenieurbüro Anlagentechnik GmbH, Arnstädter Straße 28, 99096 Erfurt, Germany

* Correspondence: Imhof@uni-koblenz.de (W.I.); wolfgang.weigand@uni-jena.de (W.W.); laithmazahreh81@gmail.com (L.R.A.)

Abstract: The electrochemical reduction of the complex [Fe$_2$(CO)$_6${μ-(SCH$_2$)$_2$GeMe$_2$}] (**1**) under N$_2$ and CO is reported applying cyclic voltammetry. Reduction of complex **1** in CO saturated solutions prevents the possible release of CO from the dianion **1^{2-}**, while the latter reacts with additional CO forming a spectroscopically uncharacterized product **P1**. This product undergoes a reversible redox process at $E_{1/2}$ = −0.70 V (0.2 V·s^{-1}). In this report, the structure of the neutral complex **1**, isomers of dianionic form of **1**, and **P1** are described applying DFT computations. Furthermore, we propose reaction pathways for H$_2$ production on the basis of the cyclic voltammetry of complex **1** in presence of the strong acid CF$_3$SO$_3$H.

1. Introduction

Hydrogen (H$_2$) has shown its potential to act as an alternative energy resource with a high energy density [1]. Moreover, hydrogen is an important starting material for the synthesis of fertilizers (e.g., potassium nitrate or ammonium nitrate production), where ammonia is produced via the Haber-Bosch process [2]. The cleanest way to produce H$_2$ is via water electrolysis using platinum as catalyst [3]. The latter is both rare and expensive, limiting its usefulness in large-scale energy storage [4]. In microbes, production and oxidation of hydrogen are catalyzed under ambient conditions with high efficiency and low energy features through enzymes called [FeFe]-hydrogenases [5–10] containing a [Fe$_2$S$_2$] cluster exhibiting a bridging dithiolato ligand as well as cyanido and carbonyl ligands, the so-called H-cluster, which is the active site being responsible for the catalytic process (Figure 1a) [11–16]. A detailed understanding of the catalytic mechanism of these enzymes has been of great interest to date and is an important subject of research [17–20].

(a)　　　　　　　　　　　　　　　　　　　**(b)**
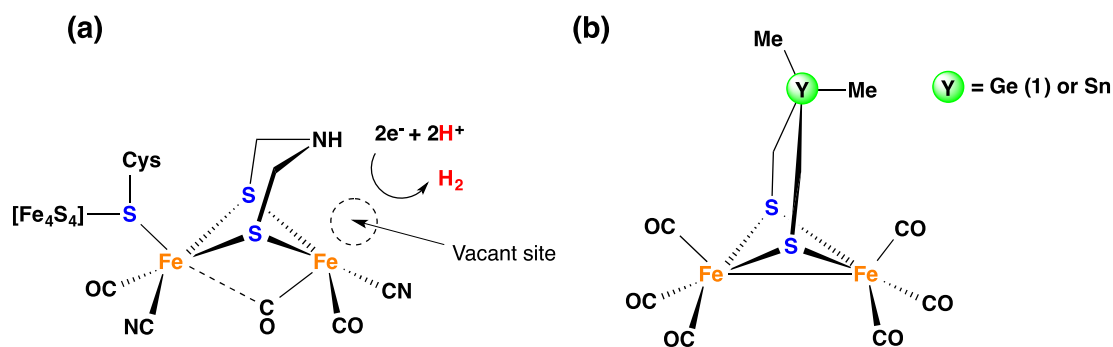
Figure 1. (**a**) The H-cluster of the [FeFe]-Hydrogenase. (**b**) Mimics of the H-cluster containing heavier group 14 atoms at the bridgehead position (Y) of the dithiolato ligand [–SCH$_2$YCH$_2$S–] (Y = GeMe$_2$ (complex **1**) or SnMe$_2$).

Until now, the catalytic mechanism for H$_2$ evolution by the H-cluster remains a subject of discussions. Nevertheless, several mechanisms were proposed based on EPR, Mössbauer spectroscopy, pH dependent FTIR spectro-electrochemistry, and DFT calculations [17–20]. Moreover, numerous hexacarbonyl diiron dithiolato complexes showing structures similar to the H-cluster were synthesize and characterized, and their catalytic applications were studied in detail in order to obtain a deeper insight into the electronic and structural characteristics of the [Fe$_2$S$_2$] core of the H-cluster and to reach a better understanding of the factors stabilizing its rotated state [21–40]. The rotated state of the H-cluster offers a vacant site (Figure 1a) at which protons or H$_2$ interact in the catalytic proton reduction or H$_2$ oxidation [17–20].

We are very keen to learn more about the influence of the nature of the dithiolato ligand on the physical and electrochemical properties of the diiron core in [FeFe]-hydrogenase mimics. In two recent papers, we found that the introduction of the heavier group 14 atoms at the bridgehead position (Y) of [-XCH$_2$YCH$_2$X-] (X = S or Se and Y = GeMe$_2$ or SnMe$_2$) ligands results in an almost planar structure of the –SCYCS– moiety for Y = GeMe$_2$ (complex **1**) or SnMe$_2$ (Figure 1b) [35]. Our previous work showed that the electron density of the μ-S atoms increases (and, consequently, that of Fe–Fe bond) [22] on going from CMe$_2$ to SiMe$_2$ to GeMe$_2$ to SnMe$_2$. As a consequence, protonation of the Fe–Fe bond is already possible using the moderately strong acid CF$_3$CO$_2$H in the case of Y = SnMe$_2$ and X = Se [38].

In continuation of our research on the influence of heteroatoms toward the structural and electrochemical properties of the model complexes [Fe$_2$(CO)$_6${μ-(SCH$_2$)$_2$Y}], we describe herein the electrochemical behavior of complex **1** (Y = GeMe$_2$) in the absence and presence of CF$_3$SO$_3$H. Furthermore, DFT computations on complex **1** and its reduction products are described.

2. Results and Discussion

The cyclic voltammogram of [Fe$_2$(CO)$_6${μ-(SCH$_2$)$_2$GeMe$_2$}] (**1**) in CH$_2$Cl$_2$/NBu$_4$PF$_6$ under N$_2$ atmosphere exhibits two reduction processes at 0.2 V·s^{-1}: A partially reversible wave at half-wave potential $E_{1/2} \approx -1.67$ V and an irreversible (irr.) wave at -1.85 V [35]. We previously proposed that the first reduction event arises from an ECE process (E = Electron transfer and C = Chemical process), whereas the second cathodic wave is due to reduction of a follow-up reaction product [35]. The follow-up reaction may involve loss of a CO ligand from the reduced species of complex **1**, as it was found for other diiron hexacarbonyl complexes [41]. Thus, we performed the experiments using a CO saturated solution to prevent CO loss from the reduced species. The corresponding results are depicted in Figure 2.
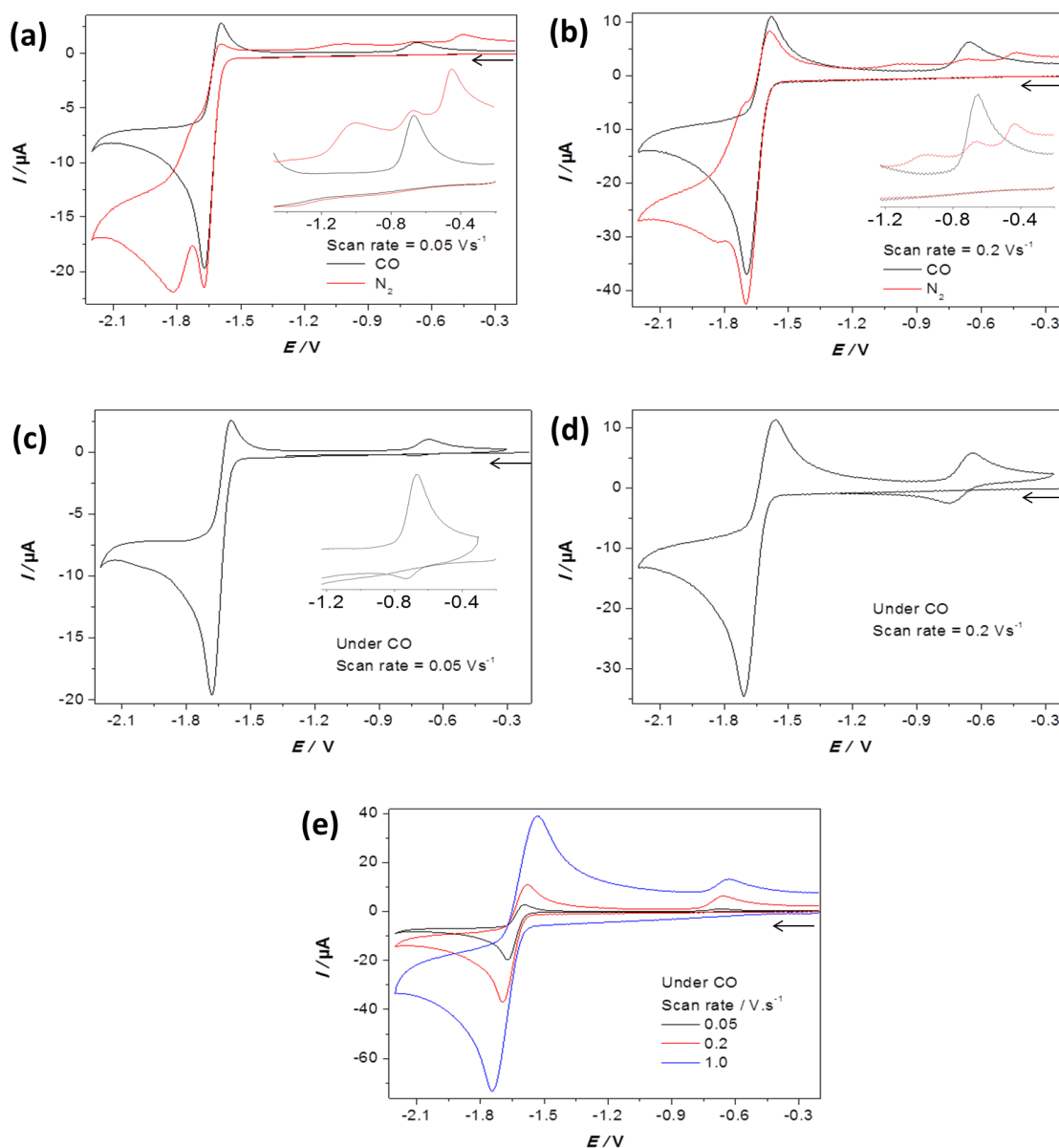
Figure 2. Cyclic voltammetry of 0.843 mM complex **1** in CH_2Cl_2/NBu_4PF_6 under conditions shown in the inset of each panels (**a**–**e**). Part of the voltammograms (**a**–**c**) are enlarged and shown in the inset for clarification. Glassy carbon electrode (diameter = 3 mm). Potential, *E*, is in volt (V) against the ferrocenium/ferrocene couple. The arrows indicate the scan direction.

The second reduction wave at −1.85 V is not observed, even at slow scan rates, if the solution of complex **1** is CO saturated (Figure 2a,b). This observation clearly indicates that the CO saturated solution effectively inhibits the loss of CO ligands from the reduced species of complex **1**, hence preventing the formation of the follow-up reaction product. As a consequence, it would be expected that the reduction of complex **1** should become reversible. However, we can notice in Figure 2a,b that the reversibility is enhanced only very slightly. In addition, only one oxidation wave occurs at −0.67 V ($\nu = 0.05$ V·s^{-1}) or at −0.64 V ($\nu = 0.2$ V·s^{-1}) when the experiment is performed using CO-saturated solutions of complex **1**. This oxidation event is also detected when the cyclic voltammetry is performed under N_2, but it co-occurs with other oxidation processes (see the insets of Figure 2a,b). Thus, the presence of CO in the solution of complex **1** inhibits the follow-up reaction occurring under N_2, but a reaction between the dianion **1**$^{2-}$ and CO takes place leading to a spectroscopically uncharacterized product **P1**. The formation of **P1** is responsible for the oxidation wave at −0.64 V ($\nu = 0.2$ V·s^{-1}).

Figure 2d shows that the oxidation of **P1** (producing another product **P2**) is a reversible process with $E_{1/2} = -0.70$ V ($E_{pc} = -0.75$ V and $E_{pa} = -0.64$ V). This behavior was also described for the complex $[Fe_2(CO)_5P(OEt)_3\{\mu\text{-}(S_2CH_2)_2(Ph)P = O\}]$ [42]. Scheme 1 summarizes the electrochemical reactions of complex **1** under N_2 as well as CO atmospheres. To gain insights into the structure of **P2**, we performed DFT calculations on the two-electron reduction of complex **1** and subsequently on the reaction between the dianionic species $\mathbf{1^{2-}}$ and CO.
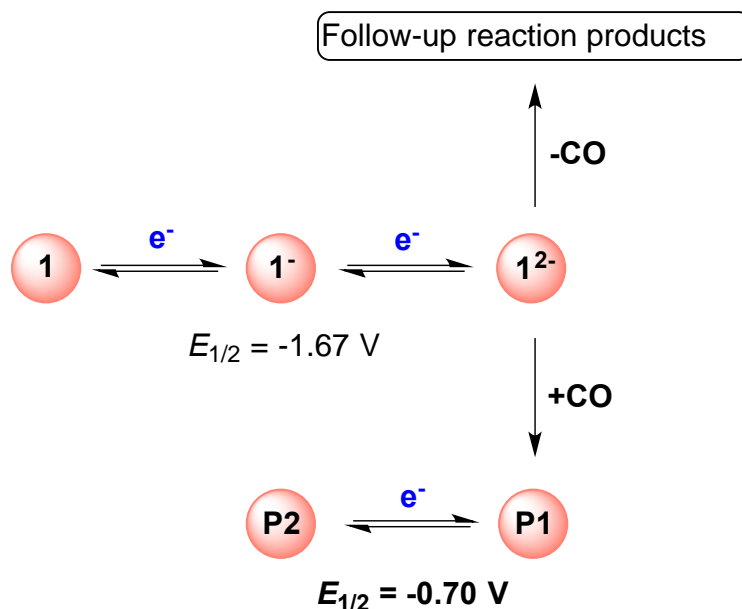
Scheme 1. Electrochemistry of complex **1** under N_2 and CO atmospheres.

## 2.1. DFT Calculations on the Reduction of Complex **1**

High-level DFT calculations were performed on the neutral dinuclear iron dithiolato complex **1** as well as on the corresponding doubly reduced species. Previous DFT computations on doubly reduced species of diiron dithiolato complexes considered two possible isomers: (1) A symmetrical dianion in which the Fe–Fe bond is broken, and (2) a rearranged dianion in which the dithiolato ligand is not symmetrically coordinated to the diiron hexacarbonyl moiety [29,42]. One major aspect of these calculations was the question of whether a rearranged structure of the dianion is thermodynamically more stable than the symmetrical isomer. In addition, we also calculated a structure of another dianion, where another CO ligand was added, and which might correspond to species **P1** that is formed under CO atmosphere. Calculations were performed applying the B3LYP/6-311++G (d,p) functional and basis set as it is implemented in *Gaussian09* [43–47]. Moreover, relativistic ECPs of the Stuttgart-Dresden group were used for iron and germanium atoms [46,47]. As the addition of CO represents a bimolecular reaction, thermal and entropic corrections were considered. It also turned out that the use of a continuum solvent model for CH_2Cl_2 was crucial to obtain results that correspond to the experimental outcome of the electrochemical investigations [48,49]. All energy values E_{corr} as well as the results of frequency calculations are summarized in Table S1 (Supplementary material), where E_{corr} corresponds to the abovementioned thermal and entropic corrections. Vibrational analysis for all calculated molecules shows that they represent minimum structures on the hypersurface (numbers of imaginary frequencies, NImag = 0).

Table 1 summarizes selected bond lengths of the calculated compounds. The molecular structures are depicted in Figure 3. From the data, it can be seen that in **1**, $\mathbf{1^-}$, and $\mathbf{1^{2-}}$, the dithiolato ligand symmetrically coordinates the two iron atoms with both sulphur atoms acting as bridging atoms. As it is expected, the iron–iron bond distance is elongated upon reduction from 253.0 pm in **1** via 287.7 pm in $\mathbf{1^-}$ to 350.2 pm in $\mathbf{1^{2-}}$. In addition, the angle between the Fe–Fe–S planes is reduced

from the typical butterfly geometry in **1** with the corresponding angle being calculated to 67.04° via 58.63° in **1⁻** to 37.70° in **1²⁻**. According to our DFT calculations, the rearranged isomer **1²⁻ (isomer)** is slightly stabilized with respect to **1²⁻** by 4.7 kJ/mol. In **1²⁻ (isomer)**, one of the sulphur atoms symmetrically bridges the two iron atoms, which now show a distance of 271.6 pm. The second sulfur atom coordinates only one of the iron atoms. In addition, there is one CO ligand that shows a semi-bridging coordination mode in the rearranged structure **1²⁻ (isomer)**. The addition of another CO ligand to **1²⁻ (isomer)** is slightly endothermic (+3.0 kJ/mol) and leads to **P1**. Nevertheless, no excess of CO was considered in the calculation of the free energy of the addition of CO to **1²⁻ (isomer)**. In **P1**, a $Fe(CO)_4$ moiety and a $Fe(CO)_3S_2$ subunit are connected by a weak iron–iron contact (306.0 pm). This interaction produces a distorted trigonal bipyramidal coordination sphere for Fe2 and a distorted octahedral environment for Fe1. Figure 4 shows the highest occupied molecular orbital, HOMO, of the respective compound, and it can be seen that a weak interaction of the two dz^2 orbitals of the iron atoms is supported by three semi-bridging CO ligands and two lone pairs at the thiolato ligand. Indeed, an analogous structure to **P1** has been proposed by DFT calculations for the product from the reaction between the dianion of $[Fe_2(CO)_5P(OEt)_3\{\mu\text{-}(S_2CH_2)_2(Ph)P = O\}]$ and CO [42].

Table 1. Selected bond lengths and distances (pm) of calculated species.

	1	**1⁻**	**1²⁻**	**1²⁻ (Isomer)**	**P₁**
Fe1–Fe2	235.0	287.7	350.2	271.6	306.0
Fe1–S1	231.3	236.4	241.8	233.2	-
Fe1–S2	231.3	235.9	239.9	-	-
Fe2–S1	231.8	235.8	240.0	234.9	245.1
Fe2–S2	231.8	236.9	242.1	243.6	241.3
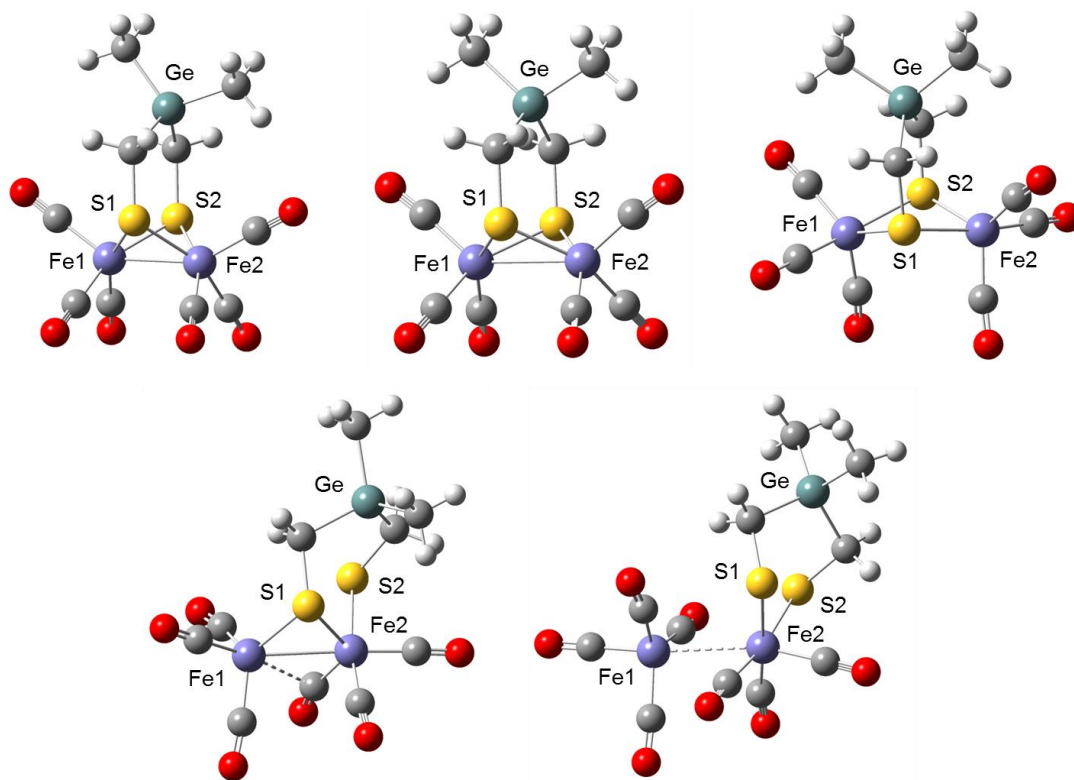
**Figure 3.** Calculated molecular structures of **1** (upper left), **1⁻** (upper middle), **1²⁻** (upper right), **1²⁻ (isomer)** (lower left), and **P₁** (lower right).
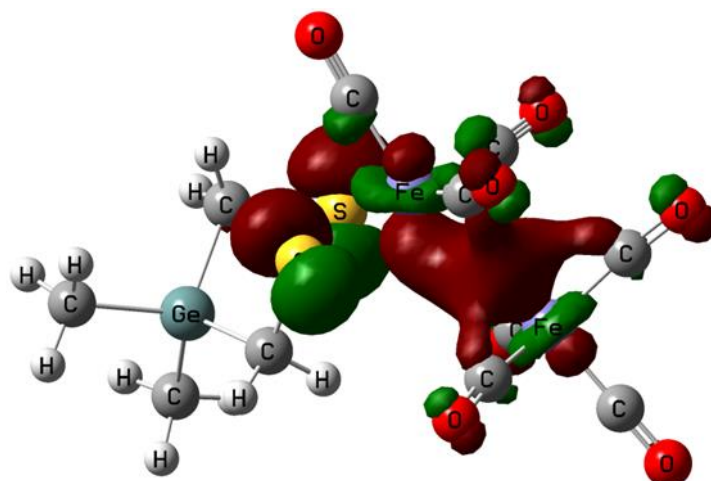
**Figure 4.** Highest occupied molecular orbital, HOMO, of **P1**.

*2.2. Electrochemical Reduction of **1** in the Presence of CF$_3$SO$_3$H*

The results of electrochemical investigations on the behavior of complex **1** in the presence of CF$_3$SO$_3$H (pK_a^{DCE} = −11.4, DCE = dichloroethane) [50] are shown in Figure 5. We only show results for 0.5–2 equiv. of CF$_3$SO$_3$H with respect to **1**, since a significant reduction of this strong acid takes place at higher concentrations. In the presence of 0.5 equiv. of CF$_3$SO$_3$H, only a shoulder at the original reduction wave of **1** (E_{pc} = −1.71 V at 0.2 V·s^{-1}) is observed at −1.60 V. This shoulder is shifted by 110 mV from the two-electron wave in the absence of CF$_3$SO$_3$H and it is attributed to the protonation of the reduced species of complex **1** affording **1H$^-$** (Scheme 2). If the concentration of CF$_3$SO$_3$H is increased, the current of the shoulder is shifted to a value that is be comparable to that of the reduction wave in the absence of acid, but without a further increase of its intensity. This suggests that there is no catalytic H$_2$-production at this potential. The cyclic voltammograms exhibit two additional waves (at −1.74 V and −2.07 V) in the presence of CF$_3$SO$_3$H, which show an increase in the current in response to increasing acid concentration. We attribute the wave at −2.07 V, which is observed at one or more equiv. of CF$_3$SO$_3$H, to the reduction of **1H$^-$** giving **1H^{2-}**. The release of H$_2$ at this potential would take place upon protonation of **1H^{2-}** (Scheme 2). The other process, which is observed at −1.74 V in the presence of 2 equiv. of CF$_3$SO$_3$H, may arise from reduction of the protonated form of **1H$^-$** (i.e., **1H$_2$**). Similar mechanisms to those shown in Scheme 2 were previously reported for other diiron dithiolato complexes [29,51].
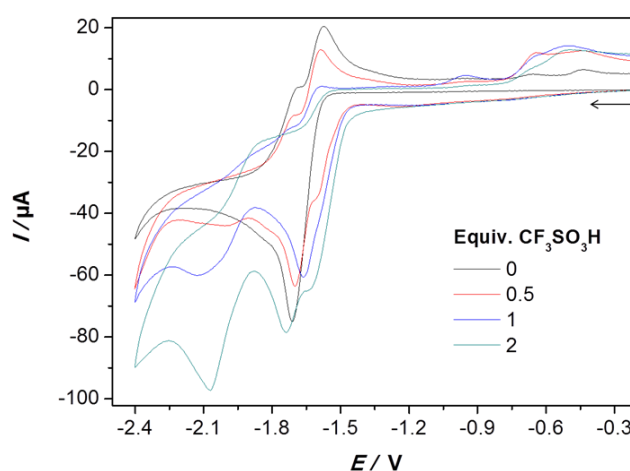
Figure 5. Cyclic voltammetry of complex 1.01 mM complex **1** (CH$_2$Cl$_2$/NBu$_4$PF$_6$) in the presence of 0.5–2 equiv. CF$_3$SO$_3$H. Glassy carbon electrode (diameter = 3 mm). Potential, *E*, is in volt (V) against the ferrocenium/ferrocene couple. The arrows indicate the scan direction.
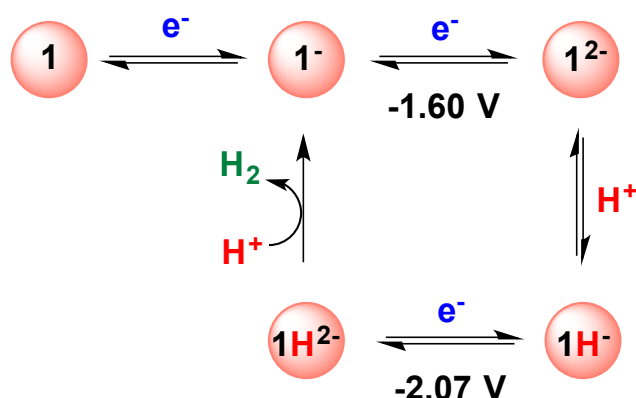
Scheme 2. Proposed reactions for the reduction of CF_3SO_3H catalyzed by complex **1**.

3. Experimental Section

3.1. Electrochemistry: Instrumentation and Procedures

These experiments do not involve corrections for the *iR* drop. Cyclic voltammetric experiments were performed in a three electrodes cell using a Radiometer potentiostat (μ-Autolab Type-III or an Autolab PGSTAT 12, Metrohm Autolab, Utrecht, Netherland) driven by the GPES software (4.9.005, Metrohm Autolab). The working electrode consisted of a vitreous carbon disk that was polished on a felt tissue with alumina before each CV scan. The Ag/Ag^+ reference electrode was separated from the analyte by a CH_2Cl_2-$[NBu_4]$ $[PF_6]$ bridge. All potentials are quoted against the ferrocene–ferrocenium couple. Ferrocene was added as an internal standard at the end of the experiments.

3.2. Theoretical Calculations

Full geometry optimizations (i.e., without symmetry constraints) were carried out with the *Gaussian09* program package using throughout the hybrid Hartree-Fock-DFT approach (B3LYP/6-311++G (d,p)) [43,46,47]. The B3LYP functional were previously found to be of suitable theoretical level for the study of iron and ruthenium carbonyl complexes [37,52–55]. For iron and germanium atoms, we used a relativistic ECP of the Stuttgart-Dresden group (SDD) [46,47]. Stationary points were rigorously characterized as minima according to the number of imaginary modes by applying a second-order derivative calculation (vibrational analysis). Zero-point energy (ZPE) corrections were applied. Solvent effects were addressed by performing a polarizable continuum model calculation for CH_2Cl_2 using the CPCM model [48,49].

4. Conclusions

The two-electron reduction of complex **1** is followed by a chemical process responsible for the irreversibility of the reduction at slow scan rates. The presence of free CO in the solution prevents this process, but CO reacts with the reduced species of **1** forming the spectroscopically uncharacterized product **P1** that undergoes a reversible redox process at $E_{1/2}$ = −0.70 V (0.2 V·s^{-1}) as shown in Scheme 1. DFT calculations show that the two-electron reduction of **1** leads to a dianionic compound **1^{2-}** which still shows a symmetrical coordination mode of the dithiolato ligand toward the diiron hexacarbonyl unit. An isomeric form of **1^{2-}**, **1^{2-} (isomer)**, is slightly more stable and, upon addition of CO, leads to a compound **P$_1$** in which a quite weak iron–iron interaction is established by the overlap of the dz^2 orbitals at both iron atoms with the delocalized π-system of three semi-bridging CO ligands and two lone pairs at the sulphur atoms. In Scheme 2, the cyclic voltammetric behavior of complex **1** in the presence of CF_3SO_3H is described, showing proposed H_2-releasing pathways.

References

1. Koroneos, C.; Dompros, A.; Roumbas, G.; Moussiopoulos, N. Life cycle assessment of hydrogen fuel production processes. *Int. J. Hydrogen Energy* **2004**, *29*, 1443–1450. [CrossRef]

2. Rauche, H. *Die Kaliindustrie im 21 Jahrhundert*; Springer: Berlin, Germany, 2015.

3. Borup, R.; Meyers, J.; Pivovar, B.; Kim, Y.S.; Mukundan, R.; Garland, N.; Myers, D.; Wilson, M.; Garzon, F.; Wood, D.; et al. Scientific Aspects of Polymer Electrolyte Fuel Cell Durability and Degradation. *Chem. Rev.* **2007**, *107*, 3904–3951. [CrossRef]

4. Ursua, A.; Gandia, L.M.; Sanchis, P. Hydrogen Production from Water Electrolysis: Current Status and Future Trends. *Proc. IEEE* **2012**, *100*, 410–426. [CrossRef]

5. Adams, M.W. The Structure and Mechanism of Iron-Hydrogenases. *Biochim. Biophys. Acta Bioenergy* **1990**, *1020*, 115–145. [CrossRef]

6. Frey, M. Hydrogenases: Hydrogen-Activating Enzyme. *ChemBioChem* **2002**, *3*, 153–160. [CrossRef]

7. Evans, D.J.; Pickett, C.J. Chemistry and the Hydrogenases. *Chem. Soc. Rev.* **2003**, *32*, 268–275. [CrossRef]

8. Volbeda, A.; Fontecilla-Camps, J.C. Structure-Function Relationships of Nickel-Iron Sites in Hydrogenase and a Comparison with the Active Sites of Other Nickel-Iron Enzymes. *Coord. Chem. Rev.* **2005**, *249*, 1609–1619. [CrossRef]

9. Fontecilla-Camps, J.C.; Volbeda, A.; Cavazza, C.; Nicolet, Y. Structure/Function Relationships of [NiFe]- and [FeFe]-Hydrogenases. *Chem. Rev.* **2007**, *107*, 4273–4303. [CrossRef] [PubMed]

10. Lubitz, W.; Ogata, H.; Rüdiger, O.; Reijerse, E. Hydrogenases. *Chem. Rev.* **2014**, *114*, 4081–4148. [CrossRef]

11. Adamska-Venkatesh, A.; Roy, S.; Siebel, J.F.; Simmons, T.R.; Fontecave, M.; Artero, V.; Reijerse, E.; Lubitz, W. Spectroscopic Characterization of the Bridging Amine in the Active Site of [FeFe] Hydrogenase Using Isotopologues of the H-Cluster. *J. Am. Chem. Soc.* **2015**, *137*, 12744–12747. [CrossRef]

12. Adamska, A.; Silakov, A.; Lambertz, C.; Rüdiger, O.; Happe, T.; Reijerse, E.; Lubitz, W. Identification and Characterization of the "Super-Reduced" State of the H-Cluster in [FeFe] Hydrogenase: A New Building Block for the Catalytic Cycle? *Angew. Chem. Int. Ed.* **2012**, *51*, 11458–11462. [CrossRef] [PubMed]

13. Fan, H.-J.; Hall, M.B. A Capable Bridging Ligand for Fe-Only Hydrogenase: Density Functional Calculations of a Low-Energy Route for Heterolytic Cleavage and Formation of Dihydrogen. *J. Am. Chem. Soc.* **2001**, *123*, 3828–3829. [CrossRef] [PubMed]

14. Peters, J.W.; Lanzilotta, W.N.; Lemon, B.J.; Seefeldt, L.C. X-ray Crystal Structure of the Fe-Only Hydrogenase (CpI) from Clostridium pasteurianum to 1.8 Angstrom Resolution. *Science* **1998**, *282*, 1853–1858. [CrossRef] [PubMed]

15. Nicolet, Y.; de Lacey, A.L.; Vernede, X.; Fernandez, V.M.; Hatchikian, E.C.; Fontecilla-Camps, J.C. Crystallographic and FTIR Spectroscopic Evidence of Changes in Fe Coordination Upon Reduction of the Active Site of the Fe-Only Hydrogenase from Desulfovibrio desulfuricans. *J. Am. Chem. Soc.* **2001**, *123*, 1596–1601. [CrossRef] [PubMed]

16. Abul-Futouh, H.; El-khateeb, M.; Görls, H.; Weigand, W. [FeFe]-hydrogenase H-cluster mimics mediated by mixed (S, Se) and (S, Te) bridging moieties: Insight into molecular structures and electrochemical characteristics. *Heteroatom Chem.* **2018**, *29*, e21446. [CrossRef]

17. De Lacey, A.L.; Fernández, V.M.; Rousset, M.; Cammack, R. Activation and Inactivation of Hydrogenase Function and the Catalytic Cycle: Spectroelectrochemical Studies. *Chem. Rev.* **2007**, *107*, 4304–4330. [CrossRef]

18. Sommer, C.; Adamska-Venkatesh, A.; Pawlak, K.; Birrell, J.A.; Rüdiger, O.; Reijerse, E.J.; Lubitz, W. Proton Coupled Electronic Rearrangement within the H-Cluster as an Essential Step in the Catalytic Cycle of [FeFe] Hydrogenases. *J. Am. Chem. Soc.* **2017**, *139*, 1440–1443. [CrossRef] [PubMed]

19. Adamska-Venkatesh, A.; Krawietz, D.; Siebel, J.; Weber, K.; Happe, T.; Reijerse, E.; Lubitz, W. New Redox States Observed in [FeFe] Hydrogenases Reveal Redox Coupling Within the H-Cluster. *J. Am. Chem. Soc.* **2014**, *136*, 11339–11346. [CrossRef]

20. Silakov, A.; Reijerse, E.J.; Albracht, S.P.J.; Hatchikian, E.C.; Lubitz, W. The Electronic Structure of the H-Cluster in the [FeFe]-Hydrogenase from *Desulfovibrio desulfuricans*: A Q-band ^{57}Fe-ENDOR and HYSCORE Study. *J. Am. Chem. Soc.* **2007**, *129*, 11447–11458. [CrossRef]

21. Li, Y.; Rauchfuss, T.B. Synthesis of Diiron(I) Dithiolato Carbonyl Complexes. *Chem. Rev.* **2016**, *116*, 7043–7077. [CrossRef]

22. Abul-Futouh, H.; Skabeev, A.; Botteri, D.; Zagranyarski, Y.; Görls, H.; Weigand, W.; Peneva, K. Toward a Tunable Synthetic [FeFe]-Hydrogenase H-Cluster Mimic Mediated by Perylene Monoimide Model Complexes: Insight into Molecular Structures and Electrochemical Characteristics. *Organometallics* **2018**, *37*, 3278–3285. [CrossRef]

23. Qian, G.; Zhong, W.; Wei, Z.; Wang, H.; Xiao, Z.; Long, L.; Liu, X. Diiron Hexacarbonyl Complexes Bearing Naphthalene-1,8-Dithiolate Bridge Moiety as Mimics of the Sub-Unit of [FeFe]-Hydrogenase: Synthesis, Characterisation and Electrochemical Investigations. *New J. Chem.* **2015**, *39*, 9752–9760. [CrossRef]

24. Figliola, C.; Male, L.; Horton, P.N.; Pitak, M.B.; Coles, S.J.; Horswell, S.L.; Grainger, R.S. [FeFe]-Hydrogenase Synthetic Mimics Based on Peri-Substituted Dichalcogenides. *Organometallics* **2014**, *33*, 4449–4460. [CrossRef]

25. Figliola, C.; Male, L.; Horswell, S.L.; Grainger, R.S. N-Derivatives of Peri-Substituted Dichalcogenide [FeFe]-Hydrogenase Mimics: Towards Photocatalytic Dyads for Hydrogen Production. *Eur. J. Inorg. Chem.* **2015**, *19*, 3146–3156. [CrossRef]

26. Samuel, A.P.S.; Co, D.T.; Stern, C.L.; Wasielewski, M.R. Ultrafast Photodriven Intramolecular Electron Transfer from a Zinc Porphyrin to a Readily Reduced Diiron Hydrogenase Model Complex. *J. Am. Chem. Soc.* **2010**, *132*, 8813–8815. [CrossRef]

27. Li, P.; Amirjalayer, S.; Hartl, F.; Lutz, M.; Bruin, B.; Becker, R.; Woutersen, S.; Reek, J.N.H. Direct Probing of Photoinduced Electron Transfer in a Self-Assembled Biomimetic [2Fe2S]-Hydrogenase Complex Using Ultrafast Vibrational Spectroscopy. *Inorg. Chem.* **2014**, *53*, 5373–5383. [CrossRef]

28. Gloaguen, F.; Morvan, D.; Capon, J.-F.; Schollhammer, P.; Talarmin, J. Electrochemical Proton Reduction at Mild Potentials by Monosubstituted Diiron Organometallic Complexes Bearing a Benzenedithiolate Bridge. *J. Electroanal. Chem.* **2007**, *603*, 15–20. [CrossRef]

29. Felton, G.A.N.; Vannucci, A.K.; Chen, J.; Lockett, L.T.; Okumura, N.; Petro, B.J.; Zakai, U.I.; Evans, D.H.; Glass, R.S.; Lichtenberger, D.L. Hydrogen Generation from Weak Acids: Electrochemical and Computational Studies of a Diiron Hydrogenase Mimic. *J. Am. Chem. Soc.* **2007**, *129*, 12521–12530. [CrossRef]

30. Schwartz, L.; Singh, P.S.; Eriksson, L.; Lomoth, R.; Ott, S. Tuning the Electronic Properties of Fe$_2$(μ-Arenedithiolate)(CO)$_{6-n}$(PMe$_3$)$_n$ (*n* = 0, 2) Complexes Related to the [Fe–Fe]-Hydrogenase Active Site. *C. R. Chim.* **2008**, *11*, 875–889. [CrossRef]

31. Capon, J.-F.; Gloaguen, F.; Schollhammer, P.; Talarmin, J. Electrochemical Proton Reduction by Thiolate-Bridged Hexacarbonyl Diiron Clusters. *J. Electroanal. Chem.* **2004**, *566*, 241–247. [CrossRef]

32. Chen, J.; Vannucci, A.K.; Mebi, C.A.; Okumura, N.; Borowski, S.C.; Swenson, M.; Lockett, L.T.; Evans, D.H.; Glass, R.S.; Lichtenberger, D.L. Synthesis of Diiron Hydrogenase Mimics Bearing Hydroquinone and Related Ligands. Electrochemical and Computational Studies of the Mechanism of Hydrogen Production and the Role of O−H···S Hydrogen Bonding. *Organometallics* **2010**, *29*, 5330–5340. [CrossRef]

33. Donovan, E.S.; McCormick, J.J.; Nichol, G.S.; Felton, G.A.N. Cyclic Voltammetric Studies of Chlorine-Substituted Diiron Benzenedithiolato Hexacarbonyl Electrocatalysts Inspired by the [FeFe]-Hydrogenase Active Site. *Organometallics* **2012**, *31*, 8067–8070. [CrossRef]

34. Felton, G.A.N.; Mebi, C.A.; Petro, B.J.; Vannucci, A.K.; Evans, D.H.; Glass, R.S.; Lichtenberger, D.L. Review of Electrochemical Studies of Complexes Containing the [Fe$_2$S$_2$] Core Characteristic of [FeFe]-Hydrogenases Including Catalysis by These Complexes of the Reduction of Acids to Form Dihydrogen. *J. Organomet. Chem.* **2009**, *694*, 2681–2699. [CrossRef]

35. Abul-Futouh, H.; Almazahreh, L.R.; Sakamoto, T.; Stessman, N.Y.T.; Lichtenberger, D.L.; Glass, R.S.; Görls, H.; El-khateeb, M.; Schollhammer, P.; Mloston, G.; et al. [FeFe]-Hydrogenase H-Cluster Mimics with Unique Planar μ-(SCH$_2$)$_2$ER$_2$ Linkers (E = Ge and Sn). *Chem. Eur. J.* **2017**, *23*, 346–359. [CrossRef] [PubMed]

36. Glass, R.S.; Gruhn, N.E.; Lorance, E.; Singh, M.S.; Stessman, N.Y.T.; Zakai, U.I. Synthesis, Gas-Phase Photoelectron Spectroscopic, and Theoretical Studies of Stannylated Dinuclear Iron Dithiolates. *Inorg. Chem.* **2005**, *44*, 5728–5737. [CrossRef] [PubMed]

37. Almazahreh, L.R.; Apfel, U.-P.; Imhof, W.; Rudolph, M.; Görls, H.; Talarmin, J.; Schollhammer, P.; El-khateeb, M.; Weigand, W. A Novel [FeFe] Hydrogenase Model with a (SCH$_2$)$_2$P=O Moiety. *Organometallics* **2013**, *32*, 4523–4530. [CrossRef]

38. Abul-Futouh, H.; El-khateeb, M.; Görls, H.; Asali, K.J.; Weigand, W. Selenium Makes the Difference: Protonation of [FeFe]-Hydrogenase Mimics with Diselenolato Ligands. *Dalton Trans.* **2017**, *46*, 2937–2947. [CrossRef]

39. Abul-Futouh, H.; Zagranyarski, Y.; Müller, C.; Schulz, M.; Kupfer, S.; Görls, H.; Elkhateeb, M.; Gräfe, S.; Dietzek, B.; Peneva, K.; et al. [FeFe]-Hydrogenase H-cluster Mimics Mediated by Naphthalene Monoimide Derivatives of Peri-Substituted Dichalcogenides. *Dalton Trans.* **2017**, *46*, 11180–11191. [CrossRef]

40. Abul-Futouh, H.; Almazahreh, L.R.; Harb, M.K.; Görls, H.; El-khateeb, M.; Weigand, W. [FeFe]-Hydrogenase H-Cluster Mimics with Various –S(CH$_2$)$_n$S– Linker Lengths (*n* = 2–8): A Systematic Study. *Inorg. Chem.* **2017**, *56*, 10437–10451. [CrossRef]

41. Trautwein, R.; Almazahreh, L.R.; Görls, H.; Weigand, W. The Influence of OH Groups in [Fe(CO)$_3$]$_2$[(μ-ECH$_2$)$_2$C(CH$_2$OH)$_2$] (E = S, Se) Complexes toward the Cathodic Process. *Z. Anorg. Allg. Chem.* **2013**, *639*, 1512–1519. [CrossRef]

42. Almazahreh, L.; Imhof, W.; Talarmin, J.; Schollhammer, P.; Görls, H.; El-Khateeb, M.; Weigand, W. Ligand Effects on the Electrochemical Behavior of [Fe$_2$(CO)$_5$(L){μ-(SCH$_2$)$_2$(Ph)P=O}] (L = PPh$_3$, P(OEt)$_3$) Hydrogenase Model Complexes. *Dalton Trans.* **2015**, *44*, 7177–7189. [CrossRef] [PubMed]

43. Frisch, M.J.; Trucks, G.W.; Schlegel, H.B.; Scuseria, G.E.; Robb, M.A.; Cheeseman, J.R.; Scalmani, G.; Barone, V.; Mennucci, B.; Petersson, G.A.; et al. *Gaussian09*; Gaussian, Inc.: Wallingford, CT, USA, 2010.

44. Becke, A.D. Density-functional thermochemistry. III. The role of exact exchange. *J. Chem. Phys.* **1993**, *98*, 5648. [CrossRef]

45. Lee, C.; Yang, W.W.; Parr, R.G. Development of the Colle-Salvetti correlation-energy formula into a functional of the electron density. *Phys. Rev.* **1988**, *B37*, 785–789. [CrossRef]

46. Dolg, M.; Stoll, H.; Preuss, H. A combination of quasirelativistic pseudopotential and ligand field calculations for lanthanoid compounds. *Theor. Chim. Acta* **1993**, *85*, 441–450. [CrossRef]

47. Bergner, A.; Dolg, M.; Küchle, W.; Stoll, H.; Preuss, H. Ab initio energy-adjusted pseudopotentials for elements of groups 13–17. *Mol. Phys.* **1993**, *80*, 1431–1441. [CrossRef]

48. Barone, V.; Cossi, M. Quantum Calculation of Molecular Energies and Energy Gradients in Solution by a Conductor Solvent Model. *J. Phys. Chem. A* **1998**, *102*, 1995–2001. [CrossRef]

49. Cossi, M.; Rega, N.; Scalmani, G.; Barone, V. Energies, structures, and electronic properties of molecules in solution with the C-PCM solvation model. *J. Comp. Chem.* **2003**, *24*, 669–681. [CrossRef] [PubMed]

50. Kütt, A.; Rodima, T.; Saame, J.; Raamat, E.; Mäemets, V.; Kaljurand, I.; Koppel, I.A.; Garlyauskayte, R.Y.; Yagupolskii, Y.L.; Yagupolskii, L.M.; et al. Equilibrium acidities of superacids. *J. Org. Chem.* **2011**, *76*, 391–395. [CrossRef]

51. Almazahreh, L.; Trautwein, R.; Görls, H.; Weigand, W. Steric effect of the dithiolato linker on the reduction mechanism of [Fe$_2$(CO)$_6${μ-(XCH$_2$)$_2$CRR′}] hydrogenase models (X = S, Se). *Dalton Trans.* **2015**, *44*, 18780–18794.

52. Peng, B.; Li, Q.S.; Xie, Y.; King, R.B.; Schaefer, H.F., III. Unsaturated trinuclear ruthenium carbonyls: Large structural differences between analogous carbonyl derivatives of the first, second, and third row transition metals. *Dalton Trans.* **2008**, 6977–6986. [CrossRef]

53. Feng, X.; Gu, J.; Xie, Y.; King, R.B.; Schaefer, H.F., III. Homoleptic Carbonyls of the Second-Row Transition Metals: Evaluation of Hartree–Fock and Density Functional Theory Methods. *J. Chem. Theory Comput.* **2007**, *3*, 1580–1587. [CrossRef] [PubMed]

54. Imhof, W.; Anders, E.; Göbel, A.; Görls, H. A Theoretical Study on the Complete Catalytic Cycle of the Hetero-Pauson-Khand-Type [2+2+1] Cycloaddition Reaction of Ketimines, Carbon Monoxide and Ethylene Catalyzed by Iron Carbonyl Complexes. *Chem. Eur. J.* **2003**, *9*, 1166–1181. [CrossRef] [PubMed]
55. Imhof, W.; Anders, E. Regioselectivity in Iron-Catalyzed [2+2+1] Cycloadditions: A DFT Investigation of Substituent Effects in 1,4-Diazabutadienes. *Chem. Eur. J.* **2004**, *10*, 5717–5729. [CrossRef] [PubMed]